EFFECT OF PREPARATION METHODS OF CeO_2-MnO_x MIXED OXIDES ON PREFERENTIAL OXIDATION OF CO IN H_2-RICH GASES OVER CuO-BASED CATALYSTS

LEI GONG[1,2], LAI-TAO LUO[1], RUI WANG[1], NING ZHANG[1,]*

[1] *Department of Chemistry, Nanchang University, Nanchang, 330031, P. R. China*
[2] *Department of Chemistry, Jiangxi Agricultural University, Nanchang, 330045, P. R. China*
(Received: August 5, 2011 - Accepted: October 3, 2011)

ABSTRACT

The CeO_2-MnO_x mixed oxides were prepared by deposition-precipitation (DP) and surfactant-templated (CB) methods, and then used as the support of CuO/CeO_2-MnO_x catalysts. The samples were characterized by means of XRD, BET, H_2-TPR, CO-TPD and XPS. Results show that preparation methods of CeO_2-MnO_x support have a direct effect on the physicochemical properties and catalytic activities of CuO/CeO_2-MnO_x catalysts for the CO preferential oxidation in H_2-rich gases(CO PROX). CuO/CeO_2-MnO_x (CB) catalyst exhibits higher CO conversion and stability in H_2-rich gases than CuO/CeO_2-MnO_x (DP), with 100% conversion of CO at 140 °C after a temperature cycle, which indicates that CeO_2-MnO_x (CB) as support of CuO based catalyst is more useful for CO PROX reaction than CeO_2-MnO_x (DP). Compared with CuO/CeO_2-MnO_x (DP), there are richer oxygen vacancies and more Mn^{4+} species on the surface of CuO/CeO_2-MnO_x (CB), and stronger interaction between CeO_2 and MnO_x in it. More amounts of active copper species and complicated transfer of electrons density on CuO/CeO_2-MnO_x (CB) also favour the activity of the catalyst.

Keywords: CuO/CeO_2-MnO_x catalyst, Preparation method of CeO_2-MnO_x, CO oxidation, In H_2-rich gases.

1. INTRODUCTION

In recent years, polymer electrolyte membrane fuel cell (PEMFC) which utilizes hydrogen as a fuel has been attracting much attention in the applications to electric vehicles or residential power-generations due to its low operation temperature, excellent energy efficiency and zero-emission of air pollutants. Hydrogen for PEMFC is generally generated from steam reforming or partial oxidation of hydrocarbons or methanol followed by the water-gas shift reaction. However, typical hydrogen mixtures from such a process usually contain 0.5-2% CO which can poison the Pt electrode in the PEMFC. Thus, carbon monoxide needs be decreased to a trace-level (below 10 ppm) to avoid poisoning of the Pt electrode. Among the current available methods to remove CO in the H_2-rich gases, preferential oxidation of CO in H_2-rich gases (PROX) was proved to be the most straightforward and economic one [1-4]. So far, extensive studies have focused on improving the activity of the catalysts for CO-PROX reaction. However, developing efficient catalysts for PROX system is still a challenge.

Catalysts for CO PROX are mainly the precious metals catalysts (such as Pt, Ru and Rh), gold-based catalysts and CuO-based catalysts [1,5]. Of these catalysts, catalysts based on combinations between copper and cerium oxides have also shown promising properties for CO PROX and constitute a more interesting alternative from an economical point of view. Extensive investigations have been carried out about the preparation methods, characterization, mechanism and testing of CuO/CeO_2 catalysts [3-8]. Some researchers reported the performance of CuO/CeO_2 catalysts was superior to that of Pt-based catalysts because of strong interactions between the copper species and the CeO_2 support [6,7]. However, most CuO/CeO_2 catalysts showed the narrow temperature window with high CO conversions and its catalytic activity strongly depended on the preparation methods [1]. Generally, the mechanism for CO PROX on CuO/CeO_2 can be regarded as a redox reaction process involving lattice oxygen and lattice vacancy, and thus metals modification is important to improve the activity of CuO/CeO_2 catalysts.

Previous investigations in CuO/(CeO, M)$_x$ catalysts field have revealed that changing the chemical composition of support with ceria-related mixed oxides (Ce-M) instead of pure CeO_2 could greatly improve the catalyst activity, which has mainly been attributed to the enhanced oxygen mobility of CeO_2-MO_x and the synergetic effect through the interaction between the mixed oxides [8]. CeO_2–MnO_x mixed oxides, as the two-way support, could exhibit much better redox properties than ceria alone due to multi-valence state and strong interaction between ceria and manganese. However, reports on CO-PROX over CeO_2-MnO_x oxides support are still less.

It is well known that catalytic activity strongly depended on not only chemical composition of catalyst, but also the preparation methods. However, to our knowledge, the effect of CeO_2-MnO_x support prepared with different methods on the activity of the CuO-based catalysts for CO-PROX has not been studied. In this work, two CeO_2-MnO_x supports were prepared by deposition-precipitation and surfactant-templated methods, respectively, and the effect of preparation methods on the performance was studied. Characterizations of the CeO_2-MnO_x or CuO/CeO_2-MnO_x were performed with N_2 adsorption, X-ray diffraction (XRD), H_2 temperature- programmed reduction (TPR), CO temperature-programmed desorption (TPD), X-ray photoelectron spectra (XPS). The results of this physicochemical characterization were discussed in relation to the exhibited catalytic performance of the CuO/CeO_2-MnO_x catalysts.

2. EXPERIMENTAL

2.1.Catalysts preparation

2.1.1. Preparation of CeO_2, MnO_x and CeO_2-MnO_x supports

Pure CeO_2 and MnO_x were prepared by precipitation method. The appropriate quantities of ammonia solution (5%) were added dropwise into the ammonium cerium(IV) nitrate solution (0.1 mol/L) and manganese(II) nitrate solution (0.1 mol/L), respectively, with vigorous stirring until pH of solution remained approximately at 10.0. The mixture was stirred for 4 h, filtered and washed with deionized water. The obtained sample was dried at 100 °C overnight and then calcined at 500 °C for 4 h under air.

CeO_2-MnO_x (DP) was prepared by deposition-precipitation method. A certain amount of ceria powder was added into the solution of 50% $Mn(NO_3)_2$ (Mn/(Mn + Ce) = 0.3, molar ratio) under vigorous stirring. Then 5% ammonia solution was added dropwise into the suspension until pH of the suspension solution was maintained at 10.0. The other steps were similar to those for the preparation of CeO_2.

CeO_2-MnO_x (CB) was prepared by surfactant-templated method. A certain amount of cetyltrimethyl ammonium bromide (CTAB, 1 mmol) as template was dissolved in 500 mL of distilled water, followed by the addition of $(NH_4)_2Ce(NO_3)_6$ and 50% $Mn(NO_3)_2$ solution (Mn/(Mn + Ce) = 0.3, molar ratio) with vigorous stirring. The other steps were similar to those for the preparation of CeO_2.

2.1.2. Preparation of CuO-based catalyst

The CuO-based catalysts were prepared by impregnation method. The as-synthesized supports were impregnated with an ethanol solution of copper nitrate for 24 h, followed by drying (100 °C; 12 h) and calcining (400 °C; 4 h). The CuO loading for CuO-based catalysts was 8.0 wt %.

2.2. Catalytic activity measurements

The CO oxidation reaction in H_2-rich gas was carried out in a continuous micro-reactor. The catalyst (0.1 g) was used. The composition of the mixture gas was 1.9 vol. % CO, 3.3 vol.% O_2, 50 vol.% H_2 and 44.8 vol.% N_2, and the space velocity was 60,000 ml/h·g. The gas composition was analyzed before and after the reaction by on-line gas chromatographs with thermal conductor detector (TCD) and carbon molecular sieve (TDX-01) column. The catalytic activity is expressed as conversion of CO. After the first measurement from 60 °C to 200 °C, the catalysts were kept at 200 °C for 10 h and decreased to room

 e-mail: nzhang.ncu@163.com

temperature, and then the second measurement was carried out from 60 °C to 200 °C to test the stabilities of the catalysts.

2.3. Characterization of the catalysts

The BET surface area and porous texture were evaluated by N_2 adsorption isotherms obtained at -196 °C using ASAP 2020 (Micrometrics) equipment. Before each measurement, the samples were degassed at 350 °C in vacuum (0.13 Pa) for 5 h. The surface area and average pore size of the samples were calculated with the BET equation and BJH formula, respectively.

The crystalline structure of the solids was studied by X-ray diffraction (XRD) using German Bruker-AXS Corporation D8 Advnce diffractometer equipped with a rotating anode, Cu Kα radiation combined with the nickel filter. Operating voltage was 40 kV and current 30 mA, with a scanning rate of 1º/min from 2θ = 20° to 80°.

H_2 temperature-programmed reduction (H_2-TPR) measurements were carried out on a Chemisorb 2750 instrument (Micrometrics). A 0.01 g sample was heated from room temperature to 600 °C under a He flow (50 ml/min) at a rate of 10 °C/min in order to remove possible impurities. After cooling to room temperature in He, a gas mixture consisting of H_2 and N_2 (10:90 *v/v*) was introduced into the system, heated to 600 °C at a rate of 10 °C /min for recording the TPR spectra.

CO temperature-programmed desorption (TPD) measurement was carried out on the same instrument with the H_2-TPR measurement. A 0.01 g sample was heated from room temperature to 400 °C under a He flow (50 ml/min) at a rate of 10 °C/min. After being cooled to room temperature, CO was injected into the reactor until adsorption was saturated. Then the sample was heated to 400 °C at a rate of 10 °C/min in He flow (50 ml/min) for recording the CO-TPD spectra.

X-ray photoelectron spectra (XPS) were determined using a KROTAS AXIS Ultra DLD spectrometer with Al Kα radiation ($h\nu$ = 1486.6 ev). The spectra of O 1s and Mn $2P_{2/3}$ levels were recorded. Charging effects were corrected by adjusting the binding energy of C 1s peak to 284.6 ev.

3. RESULTS AND DISCUSSION

3.1. The structural studies of CeO_2-MnO_x supports

The N_2-physisorption isotherms and pore size distributions of CeO_2 and CeO_2-MnO_x supports are shown in Fig. 1. Pure CeO_2 exhibits a typical type-IV isotherm with a pronounced hysteresis loop characteristics which always is connected with pore structure, and CeO_2-MnO_x (DP) exhibits a similar isotherm indicating that the pore structure is maintained. The isotherm of CeO_2-MnO_x (CB) shows a obvious difference as compared with them. The change in the shape of isotherms is probably because the Mn^{x+} ions enter ceria bulk lattice resulting in the destruction of pores. The effect of preparation method of CeO_2-MnO_x supports on the surface area (S_{BET}), pore volume (V_p), the mean pore diameter (r_p), crystallite size and cell parameter of CeO_2-MnO_x are shown in Table 1. The BET surface area of CeO_2-MnO_x (DP) is lower than that of CeO_2, probably resulting from a part ceria being covered with MnO_x during the precipitation processes. Comparing with CeO_2, CeO_2-MnO_x (CB) has larger BET surface area and smaller crystallite size, which might be due to that the CTAB template can effectively inhibit the crystal growth of CeO_2 during precipitation and calcination processes. High surface area and small crystallite size are favorable for the redox properties of the mixed oxides [9].

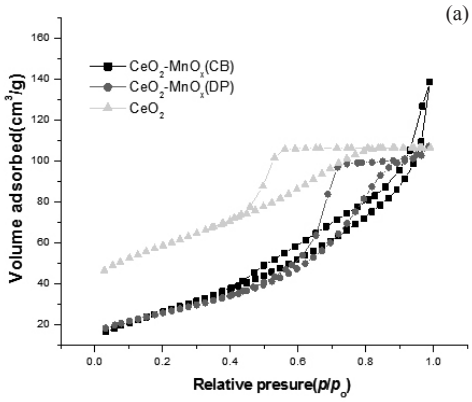

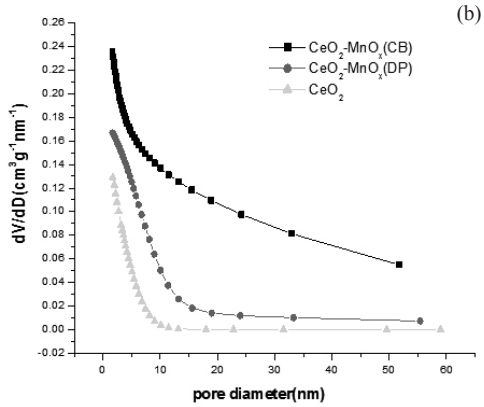

Fig. 1: N2 adsorption-desorption isotherm (a) and pore diameter distribution (b) of CeO_2 and CeO_2-MO_x supports.

Table 1: Textural characteristics of CeO_2 and CeO_2-MnO_x suppor.

Catalyst	S_{BET} ($m^2 \cdot g^{-1}$)	V_p ($cm^3 \cdot g^{-1}$)	r_p (nm)	Crystallite size (nm)[a]	Cell parameter[b]
CeO_2	140	0.14	3.4	7.7	0.5411
CeO_2-MnO_x(DP)	91.2	0.16	7.1	5.9	0.5410
CeO_2-MnO_x(CB)	148	0.24	7.6	3.6	0.5399

[a] estimated from CeO_2 (111) peak using the Scherrer formula.
[b] calculated by JADE 5.

XRD patterns of the CeO_2, MnO_x and CeO_2-MnO_x mixed oxides are shown in Fig. 1. The peaks observed at 2θ = 28.5°, 33.0°, 47.4° and 56.4° were assigned to the diffraction patterns of CeO_2 (111), (200), (220) and (311) planes, respectively. For pure MnO_x, the intensive and sharp diffractions peaks could be primarily attributed to Mn_3O_4 (PDF#24-0734). Weak diffraction peaks of MnO_x (2θ = 37.1°) is found in CeO_2-MnO_x (DP), indicating the presence of separated MnO_x, but no diffraction of MnO_x is observed in CeO_2-MnO_x (CB). Compared with pure CeO_2, the diffraction peaks of CeO_2 in CeO_2-MnO_x (CB) slightly shift to higher values of the Bragg angles and the cell parameter of that decrease obviously, which indicates the formation of solid solution of CeO_2 and MnO_x [10]. It leads to the increase of surface oxygen vacancies, as confirmed by O_2-TPD [11]. And the defect surface of solid solution can enhance the chemisorption of oxygen and accelerate the mobility of surface oxygen species [10, 12].

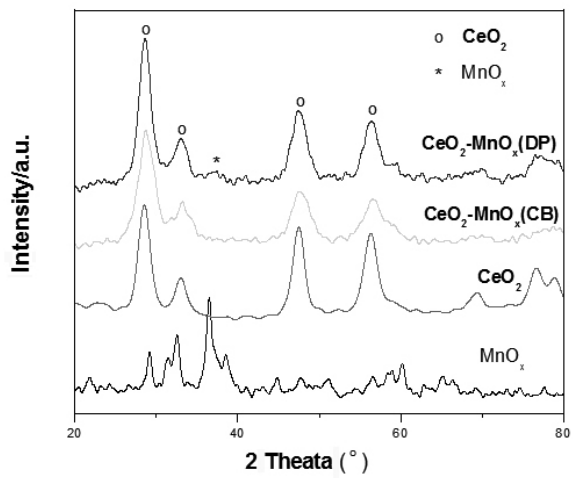

Fig. 2: XRD patterns of CeO_2, MnO_x and CeO_2-MnO_x

3.2 The reduction performance of supports and catalysts

H_2-TPR can provide information concerning the reducibility of different chemical species presented in the catalyst as well as the degree of interaction

between metal-support. The H_2-TPR profiles of CeO_2, MnO_x, CuO/CeO_2, CeO_2-MnO_x and CuO/CeO_2-MnO_x are shown in Fig. 3 and Table 2 lists the reduction temperature and hydrogen consumption of all peaks. Pure CeO_2 exhibits two reduction peaks at 380 and 780 °C, which are ascribed to the reduction of surface and bulk oxygen of CeO_2, respectively [13]. The amount of H_2 consumption is 342 $\mu mol \cdot g^{-1}$ at temperature less than 400 °C, and is about 12% of the total amount for the complete reduction of ceria from CeO_2 to Ce_2O_3. The H_2-TPR profile of pure MnO_x shows a main reduction peaks at 323 °C with a slight overlapped shoulder peak at 273 °C, indicating a two-step reduction ($MnO_x \rightarrow Mn_3O_4$ and $Mn_3O_4 \rightarrow MnO$)[14]. The total H_2 consumption is calculated to be 5103 $\mu mol \cdot g^{-1}$, from which the predominant manganese species is estimated to be Mn_3O_4 as well as some higher valence manganese oxides. It is consistent with the result of XRD. For CeO_2-MnO_x mixed oxides, the H_2-TPR profiles also show two reduction peaks (denoted as β and γ, respectively). According to the reduction characteristics of pure CeO_2 and MnO_x associated to the disappearance of the ceria low-temperature peak of CeO_2-MnO_x (CB), peak β is assigned to the reduction of $MnO_x \rightarrow Mn_3O_4$, and peak γ represents the combined reductions of $Mn_3O_4 \rightarrow MnO$ and the surface Ce^{4+}. Compared with the reduction temperature of pure MnO_x and CeO_2, the reduction temperatures of CeO_2-MnO_x (CB) at 180 and 208 °C greatly shift to lower regions, indicating the presence of interaction between manganese and cerium oxides. Although that of CeO_2-MnO_x (DP) also shift to lower temperature, the magnitude of shift is little. Thus, it can be inferred that the interaction between manganese and cerium oxides in CeO_2-MnO_x (DP) is weaker than that in CeO_2-MnO_x (CB). It is worthy noting that the H_2 consumptions of peak β is more than that of peak γ, which imply that some manganese oxide species turn to higher oxidation states in CeO_2-MnO_x (CB). All these are possibly related to the formation of CeO_2-MnO_x (CB) solid solution.

The H_2-TPR profile of CuO/CeO_2 shows two overlapped reduction peaks at 166 °C and 176 °C which should be due to the complete reductions of copper species and the surface Ce^{4+} according to the H_2 consumptions For CuO/CeO_2-MnO_x catalysts, three reduction peaks can be observed: α, β and γ. The appearance of peak α should obviously be due to the reduction of copper oxides compared with the reduction characteristics of CeO_2-MnO_x. The reduction temperature of peak α in CuO/CeO_2-MnO_x (CB) at 131 °C demonstrates a significant decrease compared with that in CuO/CeO_2 and CuO/CeO_2-MnO_x (DP). Generally, there are three kinds of copper species in CuO-CeO_2 and their reducibility follows this order [15-18]: highly dispersed Cu_xO in contact with ceria particle ＞ isolated copper ions interacting with the support ＞ large clusters and bulk CuO phase that do not contribute to the activity. According to literatures [17, 18], large clusters and bulk CuO phase are reduced at temperature higher than 200 °C; isolated copper ions interacting with the support begin to be reduced at about 160 °C; highly dispersed Cu_xO in contact with ceria is easy to be reduced at 127-160 °C. Thus, from the reduction characteristics of copper species associated to the H_2 consumption of peak α, it can be deduced that highly dispersed Cu_xO interacted with supports and isolated copper ions are the main copper species for CuO/CeO_2- MnO_x, and the amounts of highly dispersed Cu_xO in CuO/CeO_2-MnO_x (CB) are more than that in CuO/CeO_2-MnO_x (DP). In addition, the formation of CeO_2-MnO_x (CB) solid solution can facilitates the mobility of oxygen species on the surface [14], and then oxygen species can easily transfer to copper species from CeO_2-MnO_x (CB) during the reduction process. This also promote the reduction of copper species in CuO/CeO_2-MnO_x (CB) catalyst.

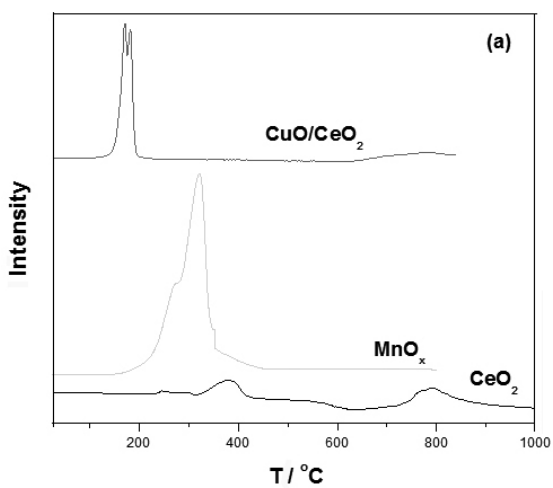

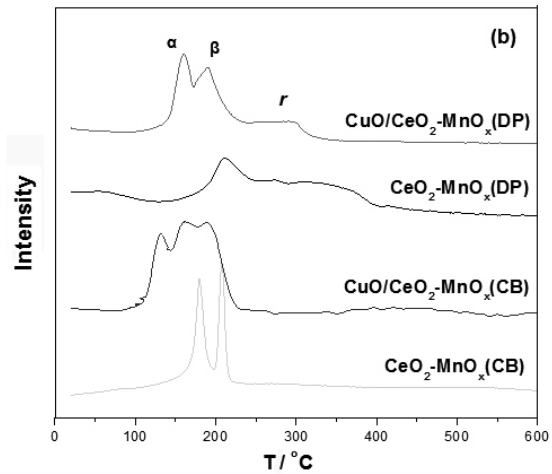

Fig. 3: H_2-TPR profiles of CeO_2, MnO_2, CuO/CeO_2 (a) and CeO_2-MnO_2, CuO/CeO_2-MnO_2 (b).

3.3 Study of XPS spectra of the catalysts

XPS characterization was performed to obtain information of the chemical state of the surface elements. Fig.4 (a) shows the XPS spectra of Mn 2p. It can be seen that the binding energy (BE) peaks of Mn $2p_{3/2}$ for CuO/CeO_2-MnO_x (DP) and CuO/MnO_x are both centered at 641.8 eV, indicting the similar state of manganese species in the two samples, and that for CuO/CeO_2-MnO_x (CB) shifts to higher binding energy centered at 642.0 eV. According to the literature [19], the BE of $Mn2p_{3/2}$ in pure manganese oxides was found to be at 641.2 eV (Mn^{2+}), 641.8 eV (Mn^{3+}) and 642.1 eV (Mn^{4+}), respectively. Then, from deconvolution of the Mn $2p_{3/2}$ peaks, it can be estimated that the relative ratio of Mn^{3+} is about 83% for CuO/CeO_2-MnO_x (DP) and that of Mn^{4+} is about 62% for CuO/CeO_2-MnO_x (CB). Therefore, the Mn^{3+} is the dominant species in CuO/CeO_2-MnO_x (DP), while Mn^{4+} ions exist in CuO/CeO_2-MnO_x (CB) as main manganese species. Six B.E peaks at 882.3, 888.8, 898.4, 900.8, 907.2 and 916.7 eV are observed in the Ce 3d XPS spectra shown in Fig.4 (b). These components should be assigned to Ce^{4+} species by comparison with the data of literatures [20]. CuO/CeO_2-MnO_x (CB) catalyst shows an inconspicuous peak at 885.0 eV along with the decrease of BE peak at 898.4 eV(arrowed in figure), which indicates the existence of Ce^{3+} species in addition to Ce^{4+}. The generation of more Mn^{4+} species with existence of partial Ce^{3+} species should be arised from the strong interaction between CeO_2 and MnO_x in CuO/CeO_2-MnO_x (CB). As is well known, high valence state of manganese oxides is easily reduced, so the presence of Mn^{4+} may enhance the redox property of the catalyst.

Fig.4 (c) shows the XPS spectra of Cu $2p_{3/2}$ in CuO-based catalysts. It can be observed that these spectra consist of the main peak of Cu $2p_{3/2}$ centered at 932.6-933.8 eV and a shake-up peak around 942.5 eV. The B.E peak of Cu $2p_{3/2}$ for CuO/CeO_2 is found at 933.8 eV with a clear shake-up peak, which is the characteristic of CuO according to the literature [21, 22]. Lower B.E at 932.2-933.1 eV and the absence of the shake-up peak are characteristic of Cu_2O [22, 23]. The Cu $2p_{3/2}$ peaks shift to lower B.E for CuO/CeO_2-MnO_x(CB), CuO/CeO_2-MnO_x(DP) and CuO/MnO_x compared with CuO/CeO_2, and CuO/CeO_2-MnO_x(CB) exhibits the lowest BE. The shift indicates some modifications of electronic properties of copper species, suggesting the occurrence of electrons transfer between copper species and manganese species. The valence state of copper species on CuO/CeO_2-MnO_x(CB) are also effected by oxygen vacancy on CeO_2-MnO_x(CB) solid solution according to U.R. Pillai's reports [24]. Simultaneously, the shift is accompanied with a obvious decrease of the intensity of the shake-up peak. Thus, their XPS spectra of Cu $2p_{3/2}$ demonstrate that Cu^+ species exist in these three catalysts, and the number of Cu^+ species on CuO/CeO_2-MnO_x (CB) seems to be more than that on CuO/CeO_2-MnO_x (DP). Cu^+ species is far likely to be the active site for CO adsorption during the CO PROX reaction [7].

Table 2: H_2 consumption amount and reduction temperature of the samples

Samples	α peak		β peak		γ peak	
	H_2 cons. ($\mu mol \cdot g^{-1}$)	Peak temp. (℃)	H_2 cons. ($\mu mol \cdot g^{-1}$)	Peak temp. (℃)	H_2 cons. ($\mu mol \cdot g^{-1}$)	Peak temp. (℃)
CeO_2	342	380	386	780	—	—
MnO_x	1146	273	3957	323	—	—
CeO_2-MnOx(DP)	–	–	578	206	723	315
CeO_2-MnOx(CB)	–	–	693	180	612	208
CuO/CeO_2	771	166	583	176	—	—
CuO/CeO_2-MnOx (DP)	806	160	1120	191	404	290
CuO/CeO_2-MnOx (CB)	845	131	802	163	723	189

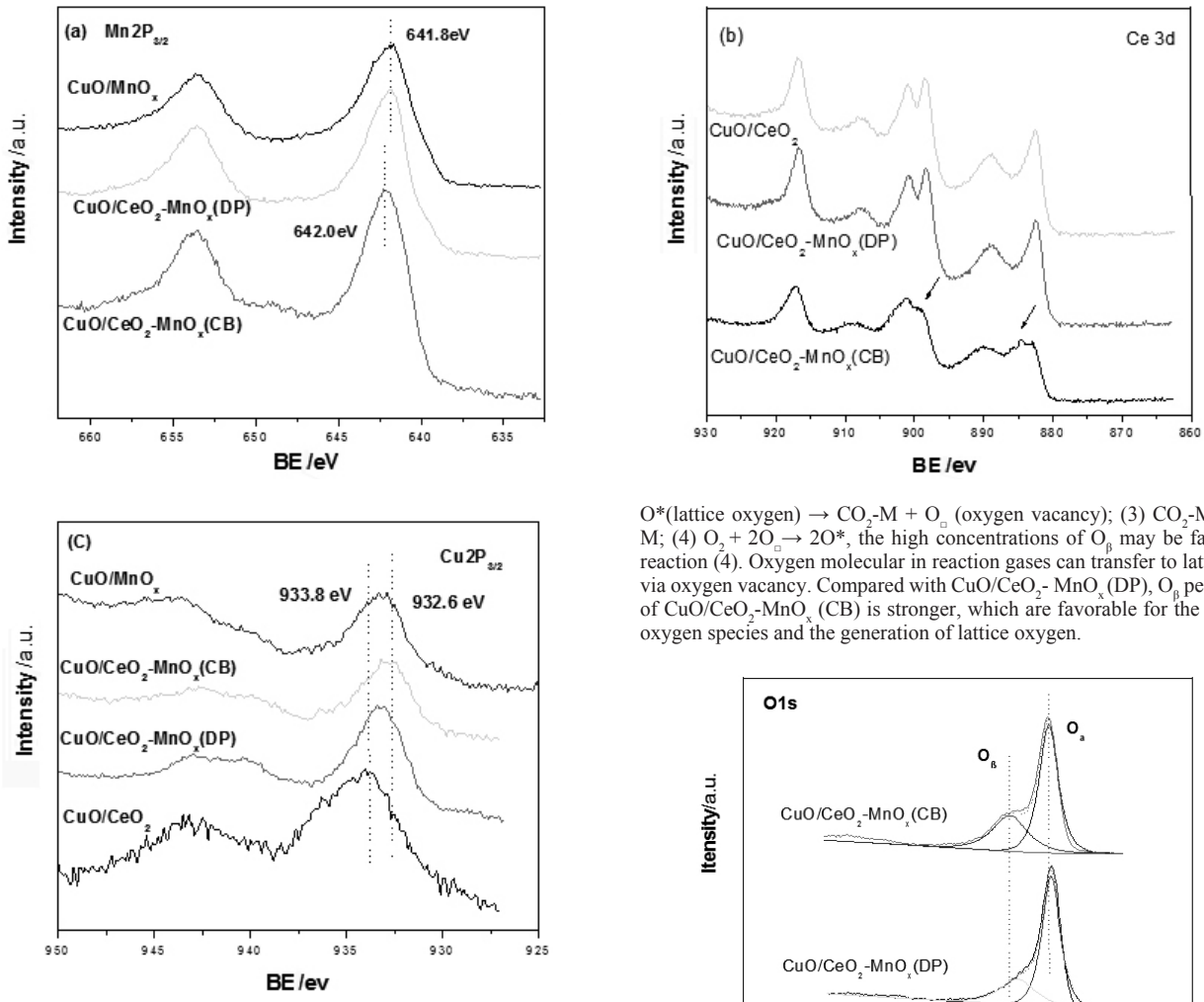

Fig. 4: XPS spectra of Mn $2p_{3/2}$ (a), Ce 3d (b) and Cu $2p_{3/2}$ (c) for catalysts.

Fig. 5 displays the XPS spectra of O1s used to investigate the oxygen species on the surface of CuO/CeO_2-MnO_x catalysts. The O1s spectra of CuO/CeO_2-MnO_x catalysts contain a main peak at 528.9-529.5 eV could be ascribed to the lattice oxygen (denoted as O_α), along with a shoulder at 531.3-532.3 eV assigned to the defect oxides or a mixture of hydroxyl groups on the surface of the catalysts (denoted as O_β) [25]. The defect oxides are favorable produce of oxygen vacancy. The comparison of the XPS spectra of O 15 between CuO/CeO_2-MnO_x (DP) and CuO/CeO_2- MnO_x (CB) indicates that the main peak intensity of the two catalysts is similar, indicating their lattice oxygen amount is almost the same. The relative concentrations of O_β listed in table 3 are 23.6 and 41.7 % for CuO/CeO_2-MnO_x (DP) and CuO/CeO_2-MnO_x (CB), respectively. According to the following mechanism of preferential oxidation of CO (PROX) [26]: (1) CO + M (adsorption site) → CO-M; (2) CO-M + O*(lattice oxygen) → CO_2-M + $O_□$ (oxygen vacancy); (3) CO_2-M → CO_2 + M; (4) $O_2 + 2O_□ \rightarrow 2O^*$, the high concentrations of O_β may be favorable for reaction (4). Oxygen molecular in reaction gases can transfer to lattice oxygen via oxygen vacancy. Compared with CuO/CeO_2- MnO_x (DP), O_β peak intensity of CuO/CeO_2-MnO_x (CB) is stronger, which are favorable for the mobility of oxygen species and the generation of lattice oxygen.

Fig. 5: XPS spectra of O1s for Cuo/CeO_2-MnO_x catalysts.

Table 3: XPS results of CuO/CeO_2–MnO_x catalysts.

Catalyst	BE(ev)		$O_\beta/(O_\alpha+O_\beta)$ (%)
	O_α	O_β	
CuO/CeO_2-MnO_x(DP)	529.4	531.8	23.6
CuO/CeO_2-MnO_x(CB)	529.5	532.1	41.7

3.4. CO adsorption property of the catalysts

CO-TPD curves of CuO/CeO_2-MnO_x catalysts are given in Fig. 5. CuO/CeO_2-MnO_x catalysts show two CO desorption peaks: α and β. CO desorption peaks temperature of CuO/CeO_2-MnO_x (DP) and CuO/CeO_2-MnO_x (CB) is 110, 175 °C and 105, 180 °C, respectively. As reported [27, 28], the CO desorption peaks are around 250 and 110 □ for pure MnO_x and CuO/CeO_2, respectively. This indicates that the peak α and β should be due to CO adsorbed on the copper species and manganese species in CuO/CeO_2-MnO_x catalysts, respectively. The α peak areas of CuO/CeO_2-MnO_x (CB) catalyst is much larger, implying that more copper active sites as CO adsorption sites exist in CuO/CeO_2-MnO_x (CB). CuO/CeO_2-MnO_x (DP) shows stronger peak β, indicating more manganese species as CO adsorption sites on its surface. The more copper species active sites and adsorption amount of CO, the more available the reactions were.

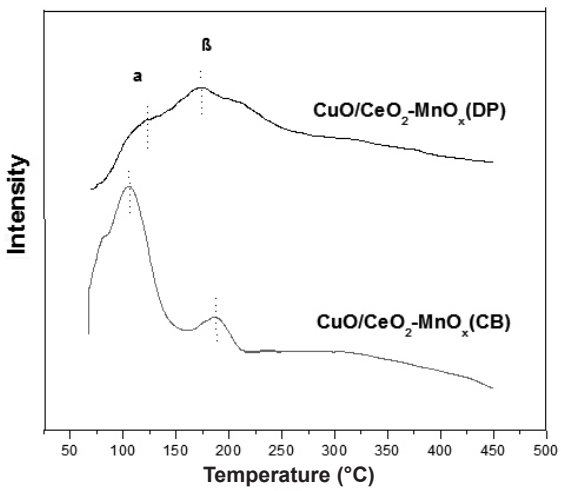

Fig. 6: CO-TPD profiles of CuO/CeO_2-MnO_x catalysts.

3.5. Performance of CuO/CeO_2-MnO_x catalysts

The catalytic activity of CeO_2-MnO_x mixed oxides and CuO-based catalysts for CO PROX system is shown in Fig. 7. CeO_2-MnO_x mixed oxides show relative low CO conversion in the temperature range investigated. It can be found that catalytic activity is not only dependent upon active constituents, but also has relations with supports of the catalysts. Obviously, the catalytic activity values of CuO-based catalysts with CeO_2-MnO_x mixed oxides as two-way support are higher than that with single support, especially at low temperature. From Fig.7, the catalytic activity of catalysts can be ranked as: CuO/CeO_2-MnO_x (CB)>CuO/CeO_2-MnO_x (DP)>CuO/CeO_2 >CuO/MnO_x. The activity of CuO/CeO_2-MnO_x (CB) catalyst is higher than that of CuO/CeO_2-MnO_x (DP). A complete conversion of CO over CuO/CeO_2-MnO_x (CB) achieves at 140 °C, whereas that over CuO/CeO_2-MnO_x (DP) catalyst is at 180 °C. This result indicates that the preparation methods of CeO_2-MnO_x support have a significant influence on the catalytic performance of CuO/CeO_2-MnO_x catalysts. After the first measurement, CuO/CeO_2-MnO_x catalysts are successively under reaction atmosphere at 200 °C for 10 h and cool down to room temperature, and then start the second activity test. The results after the temperature cycle are shown in Fig.8. It can be observed that the conversion of CO remains almost unchanged, in addition to a slight decrease at 60 °C and 80 °C. The values of CuO/CeO_2-MnO_x (CB) and CuO/CeO_2-MnO_x (DP) decrease by 6% and 10% at 80 °C, respectively. This indicates that CuO/CeO_2-MnO_x (CB) catalyst is more stable for CO oxidation in H_2-rich gases than CuO/CeO_2-MnO_x (DP).

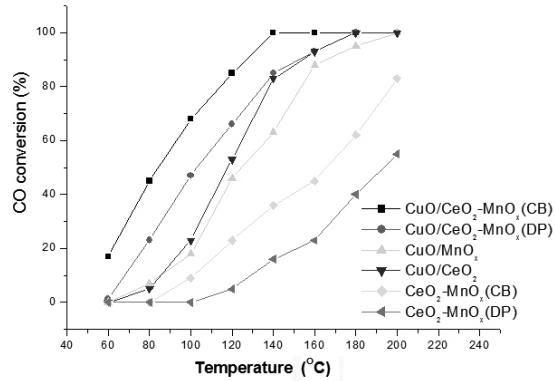

Fig. 7: The catalytic performance of CeO_2-MnO_x and CuO-based catalysts.

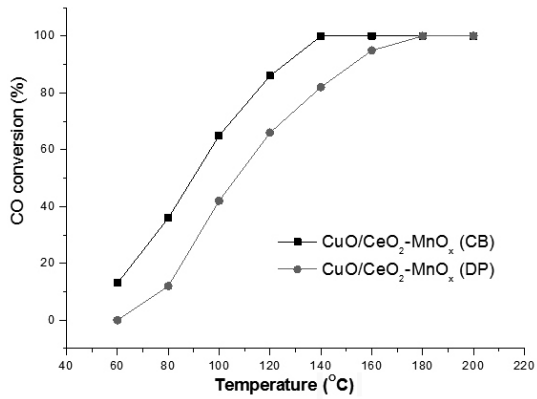

Fig. 8: Results of the second activity test over CuO/CeO_2-MnO_x catalysts.

4. CONCLUSION

In this work, CeO_2-MnO_x was prepared by deposition-precipitation (DP) and surfactant- templated (CB) methods, and then used as support of CuO/CeO_2-MnO_x catalysts. The structure analysis indicates that CeO_2-MnO_x (CB) support prepared by surfactant-templated mothd possesses a larger BET surface area and smaller particle size, compared with CeO_2-MnO_x (DP). Meanwhile, the formation of stable solid solution results in the strong interaction between CeO_2 and MnO_x in CeO_2-MnO_x (CB). The experimental results confirm that there are richer surface oxygen vacancies and more Mn^{4+} species on the surface of CuO/CeO_2-MnO_x (CB) than that of CuO/CeO_2-MnO_x (DP). Surface oxygen vacancies facilitate the transference of oxygen species from CeO_2-MnO_x (CB) to active copper species and Mn^{4+} species improve the reduction of catalyst. And there are complicated electrons transfer occurred in CuO/CeO_2-MnO_x (CB) catalyst. All these must be benefit to CuO/CeO_2-MnO_x (CB) catalyst on CO PROX reaction. In addition, the more amounts of active copper species and CO adsorption sites distributed on CeO_2-MnO_x (CB) should be responsible for the superior performance of CuO/CeO_2-MnO_x (CB) catalyst. As a result, CuO/CeO_2-MnO_x (CB) catalyst shows higher catalytic activity (CO conversion reach 100% at 140 °C) and stability than CuO/CeO_2-MnO_x (DP).

ACKNOWLEDGEMENTS

We gratefully acknowledge the financial support from the National Natural Science Foundation of China (No. 21062013).

REFERENCES

1. E. D Park, D. Lee, H. C. Lee. *Catal. Today*. 139, 280, (2009).
2. Eun-Yong Ko, EunDuck Park, KyungWon Seo. *Catal.Toda* .116, 377, (2006).
3. G.Avgouropoulos, T.Loannides, H.K.Matralis. *Catal. Lett.* 73, 33, (2001).
4. D.H.Kim, J.E.Cha. *Catal.Lett.* 86, 107, (2003).
5. Hui Wang, Huaqing Zhu, Zhangfeng Qin. *J. Catal.* 264, 154, (2009).
6. A.M.D.deFarias, A.P.M.G.Barandas, R.F.Perez, M.A.Fraga. *J. Power. Sources.* 165, 854, (2007).

7. W. Liu, MF. Stephanopoulos. *J. Catal.* 153, 304, (1995).
8. A. Martinez-Arías, A.B. Hungría, M. Fernández-García. *J. Power. Sources.* 151, 32, (2005).
9. Li Lei, Zhan Ying-Ying, Chen Chong-Qi. *Acta Phys.-Chim. Sin.* 25, 1397, (2009).
10. X.F. Tang, J.L. Chen, X.M. Huang, Y.D. Xu, W.J. Shen. *Appl. Cata. B*: *environ.* 81, 115, (2008).
11. Qing Liang, Xiaodong Wu,Duan Weng, Haibo Xu. *Catal. Today.* 139, 113, (2008).
12. Gregor Sedmak, Stanko Hočevar, Janez Levec. *J. Catal.* 213, 135, (2003).
13. Tiziana Caputo, Luciana Lisi, Raffaele Pirone, Gennaro Russo. *Appl. Cata. A*: *Genl.* 348, 42 (2008)
14. X.F. Tang, J.L. Chen, Y.G. Li, Y. Li,Y.D. Xu, W.J. Shen. *Chem. Eng. J.* 118, 119, (2006).
15. Zhigang Liu, Renxian Zhou, Xiaoming Zheng. *J. Mol. Catal. A:Chem.* 267, 137, (2007).
16. Meng-Fei Luo, Jing-Meng Ma, Ji-Qing Lu, Yu-Peng Song, Yue-Juan Wang. *J. Catal.* 246, 52, (2007).
17. Liu Y, Fu Q, M.F. Stephanopoulos. *Catal. Today.* 9, 241, (2004).
18. A.Martinez-Arias, M.Fernandez-Garcia, J. Soria, J.C. Conesa. *J. Catal.* 182, 367, (1999).
19. Kanaparthi Ramesh, Luwei Chen, Fengxi Chen, Yan Liu, Zhan Wang, Yi-Fan Han. *Catal. Today.* 131, 477, (2008).
20. Hanbo Zou, Xingfa Dong, Weiming Lin. *Appl. Surf. Sci*. 253, 2893, (2006).
21. D. Gamarra, A. Hornés, Zs. Koppány, Z. Schay, G. Munuera, J. Soria, A. Martinez-Arias. *J. Power. Sou rces.* 169, 110, (2007).
22. G. Avgouropoulos, T. Ioannides, H. Matralis. *Appl. Cata. B*: *environ.* 56, 87, (2005).
23. W. Liu , M.F. Stephanopoulos. *J. Catal.* 153, 317, (1995).
24. U.R. Pillai, S. Deevi. *Appl. Cata. B*: *environ.* 65,110, (2006).
25. Z.Y. Pu, J.Q. Lu, M.F. Luo, Y.L. Xie. *J. Phys. Chem. C.* 111, 18695, (2007).
26. Christopher S. Polster, Hari Nair, Chelsey D. Baertsch. *J. Catal.* 266, 308, (2009).
27. Xuesong Liu, Jiqing Lu, Xiaoxia Wang, Mengfei Luo. *Chin. J. Catal.* 31, 181, (2010).
28. Meng-Fei Luo, Yi-jun Zhong, Xian-xin Yuan, Xiao-Ming Zheng. *Appl. Catal. A: Gen.* 162, 121, (1997).